Chapter 6
Carbonatitic Lower-Mantle Mineral Association

Abstract In addition to ultramafic and mafic associations, a primary natrocarbonatitic association occurs in the lower mantle. To date, it was identified as inclusions in diamonds from the Juina area, Mato Grosso State, Brazil. It comprises almost 50 mineral species: carbonates, halides, fluorides, phosphates, sulphates, oxides, silicates, sulphides and native elements. In addition, volatiles are also present in this association. Among oxides, coexisting periclase and wüstite were identified, pointing to the formation of the natrocarbonatitic association at a depth greater than 2000 km. Some iron-rich (Mg,Fe)O inclusions in diamond are attributed to the lowermost mantle. The initial lower-mantle carbonatitic melt formed as a result of low-fraction partial melting of carbon-containing lower-mantle material, rich in P, F, Cl and other volatile elements at the core–mantle boundary. During ascent to the surface, the initial carbonatitic melt dissociated into two immiscible parts, a carbonate-silicate and a chloride-carbonate melt. The latter melt is parental to the natrocarbonatitic lower-mantle association. Diamonds with carbonatitic inclusions were formed in carbonatitic melts or high-density fluids.

6.1 General

In addition to oxides and other minerals comprising ultramafic and mafic associations in the lower mantle, the third mineral association was unexpectedly identified in deep Earth as being carbonatitic (Kaminsky 2012). Earlier singular grains of calcite and magnesite have been reported from both upper-mantle (Wang et al. 1996; Sobolev et al. 1997) and lower-mantle (Brenker et al. 2007) associations. Multiple finds of saline or hydrous-saline fluid inclusions in fibrous diamond (Smith 2014 and references therein) further implied the presence of carbonatitic media during the formation of diamond in the mantle. In recent years, a series of carbonatitic minerals were identified as inclusions in lower-mantle diamond from Juina in Mato Grosso State, Brazil (Wirth et al. 2009; Kaminsky et al. 2009, 2013, 2015a, 2016a), confirming the presence of carbonatitic mineral associations in deep Earth.

F.V. Kaminsky, *The Earth's Lower Mantle*, Springer Geology,
DOI 10.1007/978-3-319-55684-0_6

On the other hand, experiments under high pressure indicate a significant role of carbonatitic media in the formation of diamond. For example, 'super-deep' diamonds have been experimentally crystallized in melts of the lower mantle, diamond parental carbonate–magnesiowüstite–bridgmanite–carbon system at pressures of up to 60 GPa (Litvin et al. 2014). The following chapter is based on our recent publication (Kaminsky et al. 2016a).

6.2 Lower-Mantle Carbonatitic Association in Diamonds from the Juina Area, Brazil

6.2.1 General Characteristics

To date, almost 50 mineral species of the lower mantle carbonatitic association have been identified as inclusions in diamonds from the Juina, Mato Grosso State, Brazil (Fig. 6.1), which preserved them from various dissociation reactions that probably would have occurred during ascent to the surface. Some of the carbonatitic

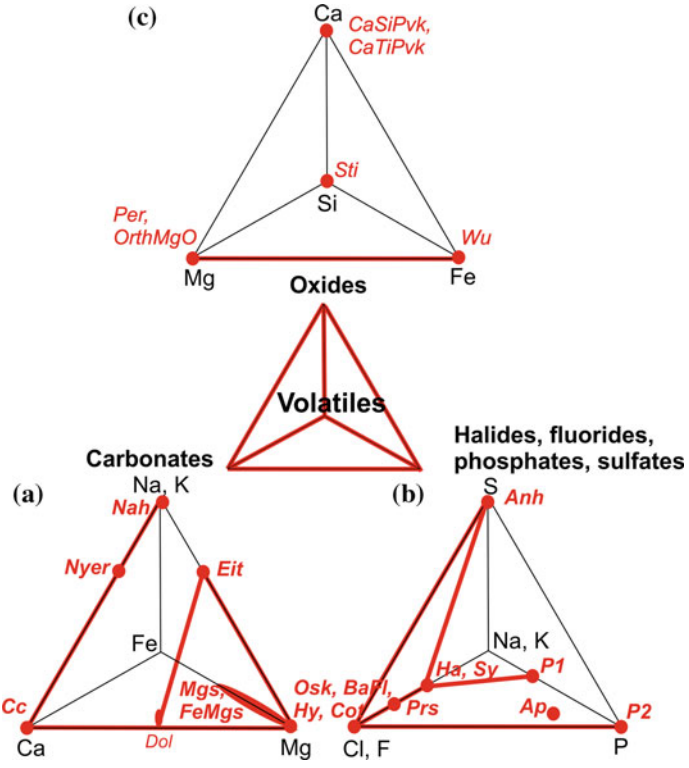

Fig. 6.1 Paragenetic associations of minerals in the primary carbonatitic association. **a** Carbonates. **b** Halides, fluorides, phosphates and sulphates. **c** Oxides. Tie *lines* are shown in *red*. Mineral indices, see Table 6.1. Modified after Kaminsky et al. (2016a). Used with a permission of Springer

Table 6.1 List of minerals of the primary carbonatitic association in the deep Earth (Kaminsky et al. 2016a)

Mineral	Index	Formula	Association	References
Carbonates				
Calcite	Cc	$CaCO_3$	CaSiPvk + CaTiPvk + Ol	Brenker et al. (2007)
			Mont + Wo II + Cusp	Wirth et al. (2009)
			Per + Wu	Kaminsky et al. (2009)
			Sp + Ap	Kaminsky et al. (2009)
			Sp + Phl(?)	
			Nyer + Wo II + CaGa	
			Nah + Phl	
			Dol + Ap + Sp + Sulf + Per + Wu + Phl(?)	Kaminsky et al. (2015a)
			$CaSiPvk + CaTiO_3 + CaMgSi_2O_6$	Zedgenizov et al. (2016)
Dolomite	Dol	$CaMg(CO_3)_2$	Ilm	Wirth et al. (2009)
			Sp + Phl	
			Cc + Ap + Sp + Sulf + Per + Wu + Phl(?)	Kaminsky et al. (2015a)
			MMgs + Eit + Ha + Sy + Phl + Pent + Vi + Sp + P1	Kaminsky et al. (2013)
Magnesite	Mgs	$Mg(CO_3)$	Dol + Eit + Ha + Sy + Phl + Pent + Vi + Sp + P1	Kaminsky et al. (2013)
			$FeMgs + Fe^0$	
Fe-magnesite	FeMgs	$(Mg,Fe)(CO_3)$	$Mgs + Fe^0$	Kaminsky et al. (2013)
Eitelite	Eit	$Na_2Mg(CO_3)_2$	Dol + Mgs + Ha + Sy + Phl + Pent + Vi + Sp + P1	Kaminsky et al. (2013)
Nyerereite	Nyer	$(Na,K)_2Ca(CO_3)_2$	Cc + Wo II + CaGa + Ap + Wu(?)	Kaminsky et al. (2009)
			Ol + Sp + Ap + Phl(?)	
Nahcolite	Nah	$NaHCO_3$	Cc + Phl	Kaminsky et al. (2009)
Halides				
Halite	Ha	NaCl	Coes + Sy + Hy + Cot + Plat + TiO_2 + Anh	Wirth et al. (2009)
			Dol + Mgs + Eit + Sy + Phl + Pent + Sp + P1	Kaminsky et al. (2015a)
			No	Kaminsky et al. (2015a)

(continued)

Table 6.1 (continued)

Mineral	Index	Formula	Association	References
Sylvite	Sy	KCl	Coes + Ha + Hy + Cot + Plat + TiO_2 + Anh	Wirth et al. (2009)
			Dol + Mgs + Eit + Ha + Phl + Pent + Vi + Sp + P1	Kaminsky et al. (2013)
Hydrophilite	Hy	$CaCl_2$	Coes + Ha + Sy + Cot + Plat + TiO_2 + Anh	Wirth et al. (2009)
Cotunnite	Cot	$PbCl_2$	Coes + Ha + Sy + Hy + Plat + TiO_2 + Anh	Wirth et al. (2009)
Fluorides				
Oskarssonite	Osk	AlF_3	P2 + BaFl	Kaminsky et al. (2013)
			SiO_2 + Fe–O + Mil	
			Hem + SiO_2	
Parascandolaite	Prs	$KMgF_3$	Hc + OrthMgO	Kaminsky et al. (2015a)
New (no name)	BaFl	$(Ba,Sr)AlF_5$	P2 + Osk	Kaminsky et al. (2013)
Sulfates				
Anhydrite	Anh	$CaSO_4$	Coes + Ha + Sy + Hy + Cot + Plat + TiO_2	Wirth et al. (2009)
Phosphates				
Apatite	Ap	$Ca_5(PO_4]_3(F,Cl)$	Nyer + Ol + Sp + Phl(?)	Kaminsky et al. (2009)
			Nyer + Cc + Wo II + Wu(?)	
			Cc + Sp + Wu	
			Cc + Dol + Sp + Sulf + Per + Wu + Phl(?)	Kaminsky et al. (2015a)
New (no name)	P1	$Na_4Mg_3(PO_4)_2(P_2O_7)$	Dol + Mgs + Eit + Ha + Sy + Phl + Pent + Vi + Sp	Kaminsky et al. (2013)
New (no name)	P2	$Fe_2Fe_5(P_2O_7)_4$	Osk + BaFl	Kaminsky et al. (2013)
Oxides				
CaSi-perovskite	CaSiPvk	$CaSiO_3$	Cc + Ol + CaTiPvk	Brenker et al. (2007)
CaTi-perovskite	CaTiPvk	$CaTiO_3$	Cc + Ol + CaSiPvk	Brenker et al. (2007)
Periclase	Per	MgO	Cc + Wu	Kaminsky et al. (2009)
			Dol + Ca + Ap + Sp + Sulf + Wu + Phl(?)	Kaminsky et al. (2015a)

(continued)

Table 6.1 (continued)

Mineral	Index	Formula	Association	References
Orrthorhombic MgO	OrthMgO	MgO	Parasc + Hc	Kaminsky et al. (2015a)
Wüstite	Wu	FeO	Cc + Per	Kaminsky et al. (2009)
			Cc + Sp + Ap	
			Nyer + Cc + Ap + Wo II	
			Dol + Ca + Ap + Sp + Sulf + Per + Phl(?)	Kaminsky et al. (2015a)
Coesite	Coes	SiO_2	Ha + Sy + Hy + Cot + Plat + TiO_2 + Anh	Wirth et al. (2009)
Non-crystalline		SiO_2	Osk + Fe–O + Mil	Kaminsky et al. (2013)
Ilmenite	Ilm	$FeTiO_3$	Dol	Wirth et al. (2009)
			Sp + Phl	
Rutile(?) (α-PbO_2 structure)	Ru(?)	TiO_2	Coes + Ha + Sy + Hy + Cot + Plat + Anh	Wirth et al. (2009)
Ilmenorutile(?)	IlmRu(?)	$(Ti,Nb,Fe)O_2$	Osk + Hem + SiO_2	Kaminsky et al. (2013)
Hematite	Hem	Fe_2O_3	Osk + SiO_2	Kaminsky et al. (2013)
Plattnerite	Plat	PbO_2	Coes + Ha + Sy + Hy + Cot + Ru + Anh	Wirth et al. (2009)
Spinel-hercynite	Hc	$FeAl_2O_4$	Parasc + OrthMgO	Kaminsky et al. (2015a)
Spinel-magnesioferrite	Sp	$(Mg,Fe)(Al,Fe)l_2O_4$	Dol + Phl + Ilm	Wirth et al. (2009)
			Nyer + Ol + Ap + Phl(?)	Kaminsky et al. (2009)
			Cc + Phl(?)	
Spinel-magnetite	Sp	Fe_3O_4	Cc + Ap	Kaminsky et al. (2009)
Spinel non-specified	Sp	Mg–Fe–Al–O	Dol + Ca + Ap + Sulf + Per + Wu + Phl(?)	Kaminsky et al. (2015a)
Silicates				
"Olivine"	Ol	$(Mg,Fe)_2SiO_4$	Cc + $CaSiO_3$ + $CaTiO_3$	Brenker et al. (2007)
			Nyer + Sp + Ap + Phl(?)	Kaminsky et al. (2009)
Wollastonite-II (high)	Wo II	$CaSiO_3$	Cc + Cusp + Mont	Wirth et al. (2009)
			Cc + Nyer + CaGa + Ap + Wu	Kaminsky et al. (2009)

(continued)

Table 6.1 (continued)

Mineral	Index	Formula	Association	References
Monticellite	Mont	$CaMgSiO_4$	Cc + Wo II + Cusp	Wirth et al. (2009)
Cuspidine	Cusp	$Ca_4(Si_2O_7](F,OH)_2$	Cc + Wo II + Mont	Wirth et al. (2009)
Ca–Garnet	CaGa	$Ca_3(Fe,Zr,Ti)_2((Si,Al)O_4]_3$	Cc + Nyer + Wo II + Ap + Wu	Kaminsky et al. (2009)
Phlogopite	Phl	$KMg_3(Si_3AlO_{10}](F,OH)_2$	Cc	Brenker et al. (2007)
			Dol + Ilm + Sp	Wirth et al. (2009)
			Nyer + Ol + Sp + Ap	Kaminsky et al. (2009)
			Cc + Sp	
			Nah + Cc	Kaminsky et al. (2009)
			Dol + Mgs + Eit + Ha + Sy + Pent + Vi + Sp + P1	Kaminsky et al. (2013)
			Dol + Ca + Ap + Sp + Sulf + Per + Wu	Kaminsky et al. (2015a)
Sulphides				
Pentlandite	Pent	$(Fe,Ni)_9S_8$	Dol + Mgs + Eit + Ha + Sy + Phl + Vi + Sp + P1	Kaminsky et al. (2013)
Violarite	Vi	$FeNi_2S_4$	Dol + Mgs + Eit + Ha + Sy + Phl + Pent + Sp + P1	
Millerite	Mil	NiS	Osk + SiO_2 + Fe–O	Kaminsky et al. (2013)
Fe(-Ni) Sulfide	Sulf	Fe–Ni–S	Dol + Ca + Ap + Sp + Per + Wu + Phl(?)	Kaminsky et al. (2015a)
Fe–Ni–Cu Sulfide	Sulf	Fe–Ni–Cu–S	(Cc + Wo II + Cusp + Mont)	Wirth et al. (2009)
Native elements				
Ni–iron	Fe^0	Fe–Ni	Mag + FeMgs	8/102 (4)

association species occur in union with lower-mantle minerals of the ultramafic association, such as ferropericlase (Kaminsky et al. 2009) and CaSi-perovskite (Brenker et al. 2007). This close association is strong evidence of their formation within the lower mantle.

The following mineral classes can be distinguished among these minerals.

1. Carbonates.
2. Halides, fluorides, phosphates and sulphates.
3. Oxides.
4. Silicates.
5. Sulphides and native elements.

In addition, volatiles are present in this association.

The first three groups of minerals are the major species. They form paragenetic associations among themselves (Fig. 6.1). The compositions of individual minerals are variable.

6.2.2 *Carbonates*

Carbonates (Fig. 6.1a) are represented by two subgroups: (a) calcite–dolomite–magnesite (including ferromagnesite, breunnerite and sideroplesite), and (b) sodium carbonates: eitelite, nyerereite and nahcolite. The minerals form paragenetic assemblages between similar cation species: calcite with nyerereite and nahcolite, and dolomite and magnesite with eitelite.

Magnesite and dolomite, in some samples, comprise the majority of the inclusions. The inclusions are euhedral in shape, which implies that it has the 'negative' morphology that is common to syngenetic mineral inclusions in diamond (Fig. 6.2). Some grains of dolomite are enriched with Fe and Mn, and are possibly ankerite (based on the observed EDX spectra).

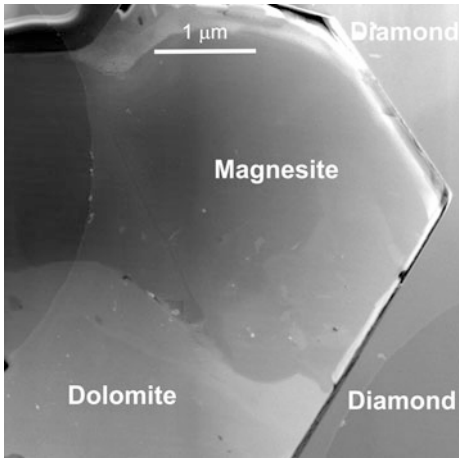

Fig. 6.2 Syngenetic inclusion of dolomite and magnesite in diamond. TEM image. Scale bar 1 μm. From Kaminsky et al. (2016a). Used with a permission of Springer

Recently, dolomite was reported as a mineral inclusion in diamond from the Machado area in Brazil, where it occurs in association with bridgmanite, ferropericlase and majorite (Burnham et al. 2016). One of the grains is dolomite with Ca/Mg close to the stoichiometry (0.967), while the other grain is, by its composition (Ca/Mg = 0.383), closer to magnesite.

Calcite occurs both as single isolated crystals, 10–30 μm in size (Kaminsky et al. 2009) and in association with other minerals (Figs. 6.1 and 6.3), including CaSi-perovskite (Brenker et al. 2007), which supports its formation within the lower mantle. Some analyzed grains contain admixtures of Sr (0.74 at.%) and Ba (trace contents), confirming their primary origin. The structure of calcite in grains associated with CaSi-perovskite was proven by both Raman spectra and X-ray diffraction (Brenker et al. 2007).

Calcite, dolomite and magnesite are primary mineral phases in the lower-mantle association (Figs. 6.2 and 6.3). This is in contrast to the occurrence of these carbonate minerals in the well-studied natrocarbonatitic lavas from the Oldoinyo Lengai, Tanzania, where calcite and dolomite (magnesite is not recorded in those lavas) are considered to have formed through transformation of the primary natrocarbonatitic association minerals (e.g., Zaitsev and Keller 2006).

Sodium carbonates are nyerereite $(Na,K)_2(Ca,Sr,Ba)(CO_3)_2$, nahcolite $NaHCO_3$ and eitelite $Na_2Mg(CO_3)_2$. Nyerereite was discovered in the early 1960s by J.B. Dawson in modern natrocarbonatitic lavas and the ashes of the Oldoinyo Lengai volcano in northern Tanzania (Dawson 1962). Nahcolite is one of the intermediate products of the hydration of nyerereite where it is widespread in altered natrocarbonatites, forming nests, veinlets and thin veins inside carbonatite flows. These minerals are characteristic for Tanzanian natrocarbonatites; in both associations (from the deep Earth and from Tanzanian volcanoes), they are similar to each other.

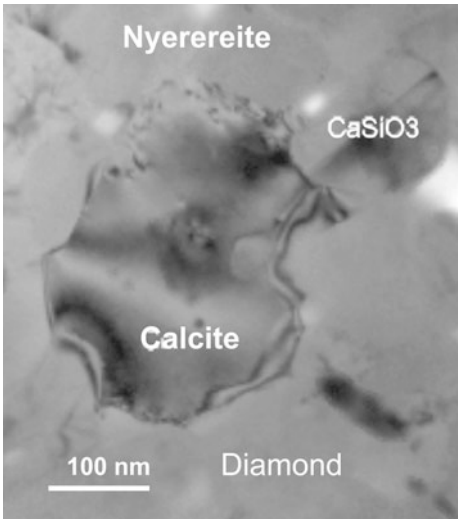

Fig. 6.3 Calcite and nyerereite in carbonatitic inclusion in diamond. TEM image. Scale bar 100 nm. From Kaminsky et al. (2016a). Used with a permission of Springer

There is no doubt that other carbonates may be found in the lower-mantle carbonatitic association. For example, tychite, sodium sulphatocarbonate $Na_6Mg_2(CO_3)_4(SO_3)$ was recently identified in mantle xenoliths from the Udachnaya-East pipe, Siberia (Sharygin et al. 2016), and potassium carbonate K_2CO_3 showed the phase transition with adopting the crystal structure of β-Na_2CO_3 under high pressure (Gavryushkin et al. 2016).

6.2.3 Halides, Fluorides, Phosphates and Sulphates

The second group of minerals is represented by a variety of compounds from volatile elements (Cl, F, P and S): halides, fluorides, phosphates and sulphates (Fig. 6.1b). Despite differences in their compositions, these minerals closely associate with one another and with the aforementioned carbonates.

Halides. In addition to the most common halides of sylvite and hydrophillite, the rare mineral of cotunnite ($PbCl_2$) also occurs. In contrast to halite and sylvite, which are typical for the Oldoinyo Lengai rocks (e.g., Zaitsev and Keller 2006), cotunnite was previously identified only as a post-volcanic (fumarole) product in active volcanoes in association with other halides, or as a secondary mineral in some lead mines. In the lower-mantle, carbonatite cotunnite associates (in addition to other halides) with another rare lead mineral, plattnerite (PbO_2).

Fluorides are another major class within this mineral group. Among them, oskarssonite (AlF_3), parascandolaite ($KMgF_3$) and a new mineral (Ba,Sr)AlF_5 were identified (Kaminsky et al. 2013, 2015a). They form assemblages in close association with phosphates.

Phosphates. Among phosphates, in addition to common apatite, two new mineral species were identified: mixed-anion ($Na_4Mg_3(PO_4)_2(P_2O_7)$ and Fe-diphosphate ($Fe_2Fe_5(P_2O_7)_4$ (Kaminsky et al. 2013). The phosphates form irregular grains in dolomite and fluoride.

Anhydrite is the only sulphate in the carbonatitic association and forms assemblages with all halides, but not with the carbonates; whereas phosphates associate with both carbonates and halides, as well as with fluorides.

6.2.4 Oxides

Oxides (Fig. 6.1c), which comprise the major part of the lower mantle, are subordinate in the carbonatitic association. Two major subgroups are distinguished within this class in the studied carbonatitic associations: (a) perovskites and (b) Mg- and Fe-oxides.

Perovskites are represented by CaSi-perovskite and CaTi-perovskite; to date, no bridgmanite has been observed. The **Mg- and Fe-oxides** do not form a compositional spectrum, unlike in the ultramafic association, where Mg-index of

ferropericlase varies from 36 to 90. By contrast, Mg- and Fe-oxides from the carbonatitic association have only 7–15 at.% Fe and 2–15 at.% Mg, respectively, and may be considered to be almost pure periclase and wüstite. Such ultimate, immiscible compositions form at high pressures, above 83–86 GPa (Dubrovinsky et al. 2000, 2001); this process is described in detail above (Sect. 4.3.3).

In addition to minerals of these two subgroups, single grains of **accessory oxides**, such as ilmenite, rutile with an α-PbO_2 structure, ilmenorutile, hematite and plattnerite (PbO_2) occur. The presence of plattnerite in association with cotunnite ($PbCl_2$) may not be accidental. Various spinel accessory varieties (hercynite, magnesioferrite and magnetite) also occur; their role is unclear.

Silica. Of particular interest is the presence of silica. In studied specimens, SiO_2 occurs in the form of coesite. However, initially it may have been stishovite or post-stishovite phases, which are unstable under decreasing pressure conditions.

6.2.5 Silicates

Silicates also occur as single grains in the carbonatitic association. Some of them (wollastonite, monticellite and cuspidine) are secondary phases, formed as a result of the decomposition of CaSi-perovskite during the ascent of the host diamond to the surface (Kaminsky et al. 2016b). A mineral phase with a composition of olivine has been identified not only in the carbonatitic association, but within the ultramafic one as well (see Sect. 4.11.1). It has not yet been studied structurally, and its nature remains unclear.

6.2.6 Sulphides and Native Iron

The other minerals, occurring in the carbonatitic association—sulphides (pentlandite, violarite and others) and native iron—belong to the matrix of the deep Earth. Native iron contains 3.5 at.% Ni (Kaminsky et al. 2013) and, in that way, is similar to meteoritic kamacite. These minerals should be considered to be accessory phases.

6.3 Natrocarbonatitic Associations

Four major types of carbonatite are known: calcite carbonatite, dolomite carbonatite, ferrocarbonatite, and natrocarbonatite (International 1989). While the first three types are distributed widely, natrocarbonatites were known only recently and in one location: as recent lavas in the Oldoinyo Lengai volcano in Tanzania (‘lengaites’; Kresten 1983), and within the Kerimasi and Tinderet carbonatites

(Mitchell 2005; Zaitsev et al. 2014). Natrocarbonatite rocks are composed mainly of nyerereite $Na_2Ca(CO_3)_2$ and gregoryite $(Na,K,Ca)_2CO_3$, with minor sylvite and fluorite in the groundmass. As such, these demonstrate comparable mineralogical and bulk chemical (Na–Cl–F) features to the carbonatitic association identified in lower-mantle Juina, Brazil, diamonds. In addition, the Juina carbonatitic association is enriched in REE, Sr and Nb, which is common for primary carbonatites. This demonstrates that the two associations, lengaite and Juina carbonatite, may be considered to be representatives of the same, natrocarbonatitic type.

There are, however, some differences in the compositions of the two associations. For example, in addition to Na-carbonates, calcite, dolomite and magnesite also occur in Juina carbonatite entrapped in diamond. Furthermore, calcite and dolomite in the lower-mantle carbonatitic association represent primary crystallizing phases, while in lengaites this mineral association is the result of the transformation of a 'primary' natrocarbonatitic association (Zaitsev and Keller 2006). Fluorite was not identified in Juina samples, while other fluorides observed in Juina are not characteristic for lengaites. Such differences may be the result of different source media compositions, their significantly differing depths of origin, and paragenesis (see Sect. 6.6).

6.4 Depth of Origin of Lower-Mantle Carbonatitic Association and the Stability of Carbonates Under Lower-Mantle Conditions

Minerals comprising the deep mantle natrocarbonatitic association are stable within a wide range of pressure–temperature (*P–T*) conditions. With the exception of secondary minerals such as monticellite, wollastonite, among others, they (or their polymorphs) are stable under conditions found within the lower mantle.

Carbonates are the major rock-forming minerals in the association. Close assemblages of carbonates with lower-mantle oxides as inclusions in diamonds from the Juina area have been identified, and include: calcite with CaSi-perovskite and $CaTiO_3$ (Brenker et al. 2007); and calcite, dolomite and nyerereite with periclase and wüstite (Kaminsky et al. 2009). The relationships between these phases and associations support an origin for the Juina natrocarbonatitic association within the lower mantle, i.e., below the 660 km discontinuity. These data agree with both experimental and theoretical data on the stability of carbonates in the deep Earth.

Magnesite is considered to be the primary carbonate phase within the deep Earth (Brenker et al. 2007; Lin et al. 2012; Scott et al. 2013). It is believed to be the most stable carbonate under conditions prevalent in the lower mantle; however ab initio calculations concluded that calcite is more stable than magnesite in the Earth's lower mantle at pressures above 100 GPa (Pickard and Needs 2015). While it has been suggested that magnesite will decompose into MgO and CO_2 at extreme pressures (Irving and Wyllie 1973) or, in association with SiO_2 into ferropericlase

with the carbon-forming diamond (e.g., Seto et al. 2008), both experimental and theoretical studies have demonstrated that it is stable under pressure conditions of up to 113–115 GPa (~2500 km depth) and T = 2100–2200 K, when magnesite $R\bar{3}c$ structure transforms into a pyroxene-type orthorhombic $MgCO_3$ ('magnesite II', Isshiki et al. 2004; Skorodumova et al. 2005; Oganov et al. 2006, 2008; Panero and Kabbes 2008), and then, at ~200 GPa from the pyroxene structure into the $CaTiO_3$ structure (Skorodumova et al. 2005). Under such extreme pressure conditions, only at very high temperatures (>2700 K) would magnesite decompose, with the formation of MgO and diamond (Solopova et al. 2015). Recently, a reaction of magnesite II with silica ($CaCl_2$-type SiO_2 or seifertite), resulting in the formation of bridgmanite and diamond was observed at pressure conditions above 80 GPa and temperatures above 1800–2000 K (Maeda et al. 2017).

Iron-containing magnesite in deep lower mantle transforms into orthorhombic $(Mg,Fe)CO_3$ phase II (Liu et al. 2015) and may form a monoclinic unusual stoichiometry $Mg_2Fe_2C_4O_{13}$ with tetrahedrally coordinated carbon (Merlini et al. 2015).

$CaCO_3$. The calculated stability of $CaCO_3$ reaches ~80 GPa pressure and T = 3300 K (Ivanov and Deutsch 2002). Within a pressure range of 1–5 GPa and T = 800–2000 K, calcite changes its rhombohedral R-3c structure to that of rhombohedral aragonite (Irving and Wyllie 1973; Ivanov and Deutsch 2002), although some triclinic (P–1) modifications ($CaCO_3$-III and, at higher pressures, $CaCO_3$-VI) are stable at pressures of up to 30 GPa (Merlini et al. 2012a, 2014; Koch-Müller et al. 2016). At pressures near 50 GPa, the aragonite orthorhombic structure undergoes a transition to a trigonal, post-aragonite structure (Santillán and Williams 2004a), and, after reaching 137 GPa (i.e., at the core–mantle boundary), the pyroxene-type $C222_1$ structure of $CaCO_3$ may be expected (Oganov et al. 2006; Ono et al. 2007). More recent ab initio random structure searching (AIRSS) suggests that in the range of 32–48 GPa another, $P2_1/c$-1 structure with sp^2 bonded carbon atoms is more stable than aragonite and post-aragonite phases; and the pyroxene-type structure with four-fold coordinated carbon atoms should be the most stable $CaCO_3$ phase at pressures from 76 GPa to well over 100 GPa (Pickard and Needs 2015).

The grain from natural sample, where calcite associates with CaSi-perovskite, was identified not only by Raman spectrum, but by XRD as well, and is demonstrated to have the calcite structure (Brenker et al. 2007). This indicates that the calcite rhombohedral structure can be stable in the natural environment and under pressure conditions of up to at least 14–24 GPa (Shim et al. 2000). In the other studied natural samples, calcite was identified by analogy on the basis of its composition only; aragonite orthorhombic or trigonal structure of some of those grains may not be excluded.

Dolomite forms a syngenetic assemblage with magnesite (Fig. 6.2; Kaminsky et al. 2013). In another sample, a spherical inclusion of wüstite + periclase in dolomite was identified, pointing to its formation under pressure conditions exceeding 86 GPa (Kaminsky et al. 2015a). This is in agreement with the experimental data of Mao et al. (2011), who demonstrated that $CaMg(CO_3)_2$ is stable under lower-mantle conditions at pressures of up to 83 GPa (and possibly higher) and contrasts with earlier data on the decomposing of dolomite into

magnesite + aragonite under lower-mantle *P–T* conditions (Biellmann et al. 1993; Luth 2001; Shirasaka et al. 2002). Recent experiments confirm that high-pressure polymorphism in dolomite could stabilize $CaMg(CO_3)_2$; this composition transforms at ~17 GPa into 'dolomite-II' (with a monoclinic structure according to Santillán et al. 2003, or an orthorhombic structure according to Mao et al. 2011, or a triclinic structure for Fe-dolomite, according to Merlini et al. 2012b) and then, at ~35–41 GPa, into 'dolomite-III' (with monoclinic structure, according to Mao et al. 2011 or a triclinic structure in the case of Fe-dolomite, according to Merlini et al. 2012a, b).

Volume differences between the three major carbonates: $CaCO_3$, $MgCO_3$ and $CaMg(CO_3)_2$ under high pressures are minimal, implying that energetic differences between these phases are small (Santillán et al. 2003) and they all may be present in the lower mantle, depending on the chemical composition of the media or within the same association under variable conditions. Among carbonates, the species with small radii of divalent cations (less than 1 Å; i.e., Mg^{2+} with 0.89 Å and Fe^{2+} with 0.78 Å radii) are more stable, while carbonates with large radii (Ca^{2+} with 1.12 Å radius) are less stable (Santillán and Williams 2004b). However, real mantle composition depends initially on the chemical composition of the media; and $CaCO_3$ and $CaMg(CO_3)_2$ may both be predominant mineral phases if the media is enriched in Ca. Rhombohedral $R\bar{3}c$-structured carbonates are the most stable under high-pressure conditions (Santillán et al. 2005); the boundary of the calcite-I to aragonite phase transition may be up to 44 GPa, as determined from $CaCO_3$ and $CdCO_3$ (Liu and Lin 1997; Santillán and Williams 2004b).

Other minerals from the natrocarbonatitic association are experimentally proven to be stable at ultrahigh-pressure conditions as well: eitelite $\geq$ 21 GPa (Kiseeva et al. 2013), parascandolaite $\geq$ 50 GPa (Aguado et al. 2008).

Of further particular interest are finds in the lower-mantle natrocarbonatitic association of almost pure periclase and wüstite. In one of the samples, two mineral species occur as coexisting, euhedral nano-inclusions in a porous carbonate matrix: periclase with Mg = 0.85–0.92 and wüstite with Mg = 0.02–0.15; no ferropericlase or magnesiowüstite of intermediate composition (which is characteristic for the oxide lower mantle) were observed (Kaminsky et al. 2009). Recently, in another sample, almost pure periclase and wüstite (with admixture of 5 wt% Fe and Mg, respectively) were observed, forming a spherical-shaped inclusion in a porous dolomite-calcite matrix: the core is composed of wüstite, and the rim is composed of periclase, both with spinel-type structures (see Fig. 4.15; Sect. 4.3.3) (Kaminsky et al. 2015a). It has been demonstrated experimentally that ferropericlase dissociates into almost pure wüstite and an Mg-rich phase at 86 GPa and 1000 K (Dubrovinsky et al. 2000, 2001). As such, the natrocarbonatitic association in the deep Earth formed at depth conditions corresponding to or exceeding 86 GPa, and corresponding to a depth in excess of 2000 km. A recent detailed study of another magnesiowüstite of composition ~$(Mg_{0.35}Fe_{0.65})O$ included in another diamond from the Juina area led to the conclusion that its origin was in one of the ultra-low

velocity zones at the base of the mantle, with this reaching the surface through diapiric upwelling culminating in kimberlite eruption (Wirth et al. 2014).

A major factor in the stability of carbonate minerals and, hence, the formation of the carbonatite association in the lower mantle is oxygen fugacity. Recent thermodynamic calculations have shown that typical values of oxygen fugacity in zones of diamond formation in the lower mantle lie between the iron–wüstite buffer and six logarithmic units above this level (Ryabchikov and Kaminsky 2013). These calculations are proven by the formation of ferropericlase in the lower-mantle within a wide range of $\Delta \log f_{O_2}$ (IW), from 1.58 to 7.76 (Kaminsky et al. 2015b). This observation makes formation of the carbonatitic association within the lower mantle realistic.

6.5 Origin of the Natrocarbonatitic Association in the Deep Earth

6.5.1 Carbon, Diamond and Hotspots

In numerous works, the presence of carbonate species in the lower mantle has been considered to be a result of the subduction of lithospheric plates and entrained sedimentary carbonates into the lower mantle (e.g., Mao et al. 2011 and references therein). An alternative explanation, however, suggests the origin of carbonate minerals in the lower mantle may instead be juvenile carbon. Deep Earth's interior is a primary reservoir for this element; it has been calculated that more than 90% of Earth's carbon is stored deep within this reservoir (e.g., Javoy 1997; McDonough 2003). The Earth's core, where the carbon content is suggested at $\sim$5 wt%, supplies carbon to the mantle over geological time via the mechanism of grain boundary diffusion that results in the formation of C–H–O volatiles (e.g., Hayden and Watson 2008). As a result, the Earth's mantle is the largest reservoir of carbon (Dasgupta and Hirschmann 2010), with an average C concentration of 100–120 ppm (Zhang and Zindler 1993; McDonough 2003).

It has been supposed, based on a series of petrologic and isotopic evidence, that carbonatite magmas may originate in the deepest parts of the mantle (Dalou et al. 2009; Bell and Simonetti 2010; Collerson et al. 2010) and be linked to the production of large igneous provinces (Ernst and Bell 2010). The data for the existence of carbonatitic inclusions in lower-mantle diamond support these ideas. It may be suggested that the formation of carbonatite and superdeep diamond initiated within the lower-mantle, in regions where hotspot/plumes occur. The observed presence of diamond in modern Hawaiian plume products, where these occur in a low-degree melt glass, rich in C, Cl, and comprising an exsolved, predominant CO_2, gas-fluid phase (Wirth and Rocholl 2003) gives a basis for such a proposition. Moreover, recent finds of carbonatitic and iron carbide-containing inclusions within the same diamond grain (Kaminsky et al. 2015a) confirm the suggestion regarding the formation of carbonatitic liquid in the deepest parts of the mantle.

'Primary', deep hotspot plumes (Courtillot et al. 2003) are thought to originate at the thermal boundary layer at the base of the lower mantle (e.g., Zhong 2006; Boschi et al. 2007). In some areas of the core–mantle boundary (CMB), anomalous seismic properties within thin zones (~10 km thick and 50–100 km wide) were identified as Ultra-Low Velocity Zones (ULVZ) due to their drop in seismic velocities greater than 10% relative to the background mantle. They are considered to be zones of partial melting, which may result from vigorous, small-scale convection or instabilities in the thermal boundary layer at the base of the mantle (Wen and Helmberger 1998; McNamara et al. 2010). ULVZ material can become entrained in mantle plumes (McNamara et al. 2010).

6.5.2 *Formation of Carbonatitic Partial Melts in the Lowermost Mantle*

The adiabatic temperature coefficient in the lower mantle was found to be 0.3 K/km (lower than in the upper mantle), and the adiabatic temperature at a depth of 2700 km was estimated at 2730 ± 50 K, if convective heat still dominates in this region (Katsura et al. 2010). However, the lower mantle is not seismically homogeneous (Bunge et al. 2001), and 3D spherical convection is not applicable to the entire deep Earth. There are data, based on the elasticity of silicate perovskite, demonstrating that the real temperature profile in the lower mantle is much steeper than the average mantle adiabatic (AMA), and below 1500 km the actual geotherm is super-adiabatic (da Silva et al. 2000). The computer simulations predict non-adiabatic excess of 100°–300° for the lower mantle because a significant proportion of mantle heat source is internal (Bunge et al. 2001). Calculations based on the measurement of perovskite shear modulus also demonstrate that lower mantle seismic properties may not match an adiabatic geotherm; geotherms may have larger temperature gradients (from 0.5 to 0.9 K/km between 800 and 2700 km), and indeed the temperature at a depth of 2700 km in some areas may reach 3400 K (Matas et al. 2007).

The pyrolite solidus temperature at the CMB was suggested to be near that of the core temperature (~3800–4000 K), suggesting possible partial melting of the lower mantle (Zerr et al. 1998). More recent experimental data on the solidus temperature at the CMB (136 GPa pressure) are even higher: 4180 ± 150 K for fertile peridotite (Fiquet et al. 2010) and 4150 ± 150 K for the chondritic composition (Andrault et al. 2011). These data are based on a study of both pyrolitic and chondritic solidi as 'dry' systems composed of only major elements (Si, Al, Fe, Ca and Mg), while the presence of alkalis and particularly C, O, H and other volatiles depress the solidus position drastically. The experimental data performed at 10–15 GPa pressure conditions demonstrated that the presence of C–O–H fluid and/or even the minor admixture of alkalis in peridotite produce carbonatitic melt at temperatures lower than adiabatic ones by as much as 400–500 °C (Litasov et al.

2013a, b; Shatskiy and Litasov 2015). It was demonstrated in experiments at up to 80 GPa, that the melting behaviour of simple carbonate systems is a suitable proxy for many carbonate-bearing lithologies (Thomson et al. 2014).

In this case, even a slight increase of temperature initiates the process of **partial melting**, which is observed in ULVZs at the CMB by P- and S-wave velocity reductions (Lay et al. 2004 and references therein). Such areas of partial melting are likely to be the roots to mantle hotspots. These hotspots are believed to be caused by the presence of chemical heterogeneities with high concentrations of fusible elements (Andrault et al. 2011). It has been calculated theoretically (Wyllie and Ryabchikov 2000), and proven experimentally (Dalton and Presnall 1998), that low-fraction melts generated near the solidus of carbon-containing mantle lherzolite at high enough oxygen fugacity values should have a carbonatite composition, with CO_2 contents of $\sim$45 wt%.

Given that estimates of the average concentrations of carbon and phosphorus in mantle peridotite are closely similar (Palme and O'Neill 2003), the *near-solidus melts should have a carbonate–phosphate composition* (Ryabchikov and Hamilton 1993a, b), exactly as is observed in the diamond-hosted Juina carbonatite association. In experiments, low-fraction volatile-rich carbonatitic melts extract many incompatible elements from parental peridotite (Ryabchikov et al. 1991). The natural carbonatite association is rich in chlorine, fluorine and other elements, which form in addition to carbonates and phosphates, fluorides and chlorides (Kaminsky et al. 2009, 2013).

As a result, carbonatitic melts can be produced from volatile- and/or alkali-rich peridotite (chondrite) at the base of the lower mantle, in the roots to mantle hotspots at the CMB.

6.5.3 *Evolution of Carbonatitic Melts in the Lower Mantle*

The suggested model for the formation and evolution of carbonatite melts in the deep Earth is illustrated in Fig. 6.4.

The **first, super-adiabatic, stage A** occurs within the lowermost mantle, starting from the CMB (D″ layer). A local increase in the thermal condition, caused most likely by processes in the upper core, triggers low-degree partial melting of lower-mantle material enriched in carbon and other volatiles. Within chambers, approximately 10–20 km thick and 50–100 km wide, carbonatitic melts containing $\geq$45 wt% CO_2 are formed. Such chambers, which are roots to future hotspots, begin to migrate upwards creating local 3D convection. Partial carbonatitic melts comprise 1–2 vol% of the mantle chamber material, and are strongly enriched in volatiles. These partial melts infiltrate mantle lithologies and percolate into regions of the mantle. Carbonate melts have been shown to be highly mobile; they can travel upward into and through the upper mantle at velocities exceeding hundreds to thousands of meters on time scales of 0.1–1 m.y.; i.e., several orders of magnitude

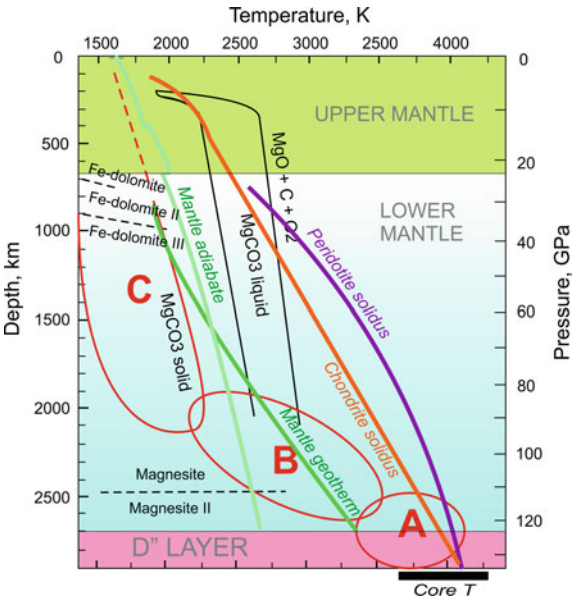

Fig. 6.4 A model for the formation and development of the carbonatitic association in the deep Earth. Modified after Kaminsky et al. (2016a). Used with a permission of Springer

higher than those previously found for basaltic liquids (Hammouda and Laporte 2000; Kono et al. 2014).

During the **second stage B**, partial melts develop at near-adiabatic conditions. During this stage, oxide phases can be crystallized; some of them may form immiscible wüstite + periclase associations under pressure values greater than 83–86 GPa (Dubrovinsky et al. 2000, 2001). The temperature conditions within this stage correspond to a multicomponent, completely miscible carbonate liquid system (Litvin et al. 2014). According to experimental data, as temperature falls, the invariant eutectic assemblage Mg–Fe–magnesite $(Mg,Fe)CO_3$ + Na-carbonate $Na_2(Mg,Fe)(CO_3)_2$ + liquid is formed (Litvin et al. 2014).

At lower *P–T* parameters, the initial carbonatitic system dissolves into two parts. Experiments at 5–16.5 GPa and high temperature demonstrated the presence of two immiscible carbonatitic systems: carbonate-silicate and chloride-carbonate (Litasov and Ohtani 2009; Safonov et al. 2011). The latter one may be considered to be an analogue to the natrocarbonatitic Juina lower-mantle association, while carbonate-silicate association has yet to be observed in mantle conditions. At high temperatures, the two immiscible liquids tend to coexist (Litasov and Ohtani 2009); however, the temperature for this immiscibility is not yet known. One may suggest that it occurs within the *P–T* conditions of the near-adiabatic stage B, where two immiscible carbonatitic melts separate. To date, only the chloride-carbonate (natrocarbonatitic) association is known, however, there is no reason to exclude the existence of the second one in the deep Earth.

Most likely, during the near-adiabatic stage B, formation of the 'ultra-deep' diamond occurs. Carbonatite media is favourable to diamond formation. It has been established experimentally that a concentration barrier of diamond nucleation

(CBDN) arises at a particular ratio of carbonate to silicate components (Litvin 2009). The CBDN position depends on the chemical composition of the system. In multicomponent silicate-carbonatite solvent, the CBDN is within the range of carbonatite compositions (<50 wt% silicates). Diamonds have been experimentally crystallized in melts of the lower-mantle diamond parental carbonate–magnesiowüstite–bridgmanite–carbon system, at conditions found within the upper part of the lower-mantle (20–30 GPa) (Litvin et al. 2014). It is apparent that admixtures of P, Cl and F within carbonatitic melt are of great importance in the formation of diamond (Palyanov et al. 2007; Sonin et al. 2008). Within both fibrous and monocrystalline upper-mantle diamonds, carbonatitic and saline high-density fluids (HDF) were identified, some of them are purely carbonatitic in composition (e.g., Schrauder and Navon 1994; Izraeli et al. 2001; Klein-BenDavid et al. 2006, 2009; Weiss et al. 2014). They are considered to be relics of diamond-forming media. The formation of lower-mantle diamonds may have happened either from carbonatitic melt or from high-density fluids.

The third stage C occurs at sub-adiabatic conditions. Various carbonate phases ($CaCO_3$, $MgCO_3$, $CaMg(CO_3)_2$ and others) form within this stage and major phase transformations occur in subsolidus conditions with the participation of remnant fluid phases. In experiments, the assemblage Mg–Fe–magnesite (Mg,Fe)CO_3 + Na-carbonate $Na_2(Mg,Fe)(CO_3)_2$, with Na_2CO_3 solidification at the lowermost isobaric temperature 1300 K (Litvin et al. 2014) was observed.

At or near to the Earth's surface, diamonds with carbonatitic inclusions are delivered, as xenocrysts, by kimberlitic volcanism. The kimberlite magmas form at shallower depth as a result of partial melting of peridotite within the upper mantle and/or transition zone. The diamonds entrained by kimberlitic magma en route to the surface are formed both in the lower mantle and upper mantle/transition zone (dominating) and, as such, contain inclusion suites of both carbonatitic and ultramafic mineral associations.

6.6 Conclusions

In addition to ultramafic and mafic associations, a primary carbonatitic association occurs in the lower mantle. It is predominantly carbonate (natrocarbonate)–halide–fluoride in composition with a minor (accessory) admixture of oxides, silicates and other minerals. It is close, by mineral composition, to the natrocarbonatitic association.

The initial lower-mantle carbonatitic melt formed as a result of low-fraction partial melting of lower-mantle material at the CMB. It was rich in P, F, Cl and other volatile elements. During ascent to the surface, the initial carbonatitic melt dissociated into two immiscible parts, a carbonate-silicate and a chloride-carbonate melt. The latter melt is parental to the observed natrocarbonatitic lower-mantle association. Diamonds with carbonatitic inclusions were formed in carbonatitic melts or high-density natrocarbonatitic fluids.

References

Aguado, F., Rodriguez, F., Hirai, S., Walsh, J. N., Lennie, A., & Redfern, S. A. T. (2008). High-pressure behaviour of $KMgF_3$ perovskites. *High Pressure Research, 28,* 539–544.

Andrault, D., Bolfan-Casanova, N., Lo Nigro, G., Bouhifd, M. A., Garbarino, G., & Mezoua, M. (2011). Solidus and liquidus profiles of chondritic mantle: Implication for melting of the Earth across its history. *Earth and Planetary Science Letters, 24,* 251–259.

Bell, K., & Simonetti, A. (2010). Source of parental melts to carbonatites—Critical isotopic constraints. *Mineralogy and Petrology, 98,* 77–89.

Biellmann, C., Gillet, P., Guyot, F., Peyronneau, J., & Reynard, B. (1993). Experimental evidence for carbonate stability in the Earth's lower mantle. *Earth and Planetary Science Letters, 118,* 31–41.

Boschi, L., Becker, T. W., & Steinberger, B. (2007). Mantle plumes: Dynamic models and seismic images. *Geochemistry, Geophysics, Geosystems, 8*(10), Q10006. doi:10.1029/2007GC001733

Brenker, F. E., Vollmer, C., Vincze, L., Vekemans, B., Szymanski, A., Janssens, K., et al. (2007). Carbonates from the lower part of transition zone or even the lower mantle. *Earth and Planetary Science Letters, 260,* 1–9.

Bunge, H.-P., Ricard, Y., & Matas, J. (2001). Non-adiabaticity in mantle convection. *Geophysical Research Letters, 28*(5), 879–882.

Burnham, A. D., Bulanova, G. P., Smith, C. B., Whitehead, S. C., Kohn, S. C., Gobbo, L., et al. (2016). Diamonds from the Machado River alluvial deposit, Rondônia, Brazil, derived from both lithospheric and sublithospheric mantle. *Lithos, 265,* 199–213. doi:10.1016/j.lithos.2016.05.022

Collerson, K. D., Williams, Q., Ewart, A. E., & Murphy, D. T. (2010). Origin of HIMU and EM-1 domains sampled by ocean island basalts, kimberlites and carbonatites: The role of CO_2-fluxed lower mantle melting in thermochemical upwellings. *Physics of the Earth and Planetary Interiors, 181,* 112–131.

Courtillot, V., Davaille, A., Besse, J., & Stock, J. (2003). Three distinct types of hotspots in the Earth's mantle. *Earth and Planetary Science Letters, 205,* 295–308.

Da Silva, C. R. S., Wentzcovitch, R. M., Patel, A., Price, G. D., & Karato, S. I. (2000). The composition and geotherm of the lower mantle: Constraints from the elasticity of silicate perovskite. *Physics of the Earth and Planetary Interiors, 118,* 103–109.

Dalou, C., Koga, K. T., Hammouda, T., & Poitrasson, F. (2009). Trace element partitioning between carbonatitic melts and mantle transition zone minerals: Implications for the source of carbonatites. *Geochimica et Cosmochimica Acta, 73,* 239–255.

Dalton, J. A., & Presnall, D. C. (1998). Carbonatitic melts along the solidus of model lherzolite in the system CaO-MgO-Al_2O_3-SiO_2-CO_2 from 3 to 7 GPa. *Contributions to Mineralogy and Petrology, 131,* 123–135.

Dasgupta, R., & Hirschmann, M. M. (2010). The deep carbon cycle and melting in Earth's interior. *Earth and Planetary Science Letters, 198*(1–2), 1–13. doi:10.1016/j.epsl.2010.06.039

Dawson, J. B. (1962). The geology of Ol Doinyo Lengai. *Bulletin of Volcanologique, 24,* 348–387.

Dubrovinsky, L. S., Dubrovinskaia, N. A., Annersten, H., Halenius, E., & Harryson, H. (2001). Stability of $(Mg_{0.5}Fe_{0.5})O$ and $(Mg_{0.8}\ Fe_{0.2})O$ magnesiowüstites in the lower mantle. *European Journal of Mineralogy, 13*(5), 857–861.

Dubrovinsky, L. S., Dubrovinskaia, N. A., Saxena, S. K., Annersten, H., Halenius, E., Harryson, H., et al. (2000). Stability of ferropericlase in the Lower Mantle. *Science, 289*(5478), 430–432.

Ernst, R. E., & Bell, K. (2010). Large igneous provinces (LIPs) and carbonatites. *Mineralogy and Petrology, 98,* 55–76.

Fiquet, G., Auzende, A. L., Siebert, J., Corgne, A., Bureau, H., Ozawa, H., et al. (2010). Melting of peridotite to 140 Gigapascals. *Science, 329,* 1516–1518. doi:10.1126/science.1192448

Gavryushkin, P.N., Rashenko, S.V., Shatskiy, A.F., Litasov, K.D., & Ancharov, A.I. (2016). Compressibility and phase transitions of potassium carbonate at pressures below 30 kbar. *Journal of Structural Chemistry*, *57*(7), 1485–1488. doi:10.1134/S0022476616070258

Hammouda, T., & Laporte, D. (2000). Ultrafast mantle impregnation by carbonatite melts. *Geology, 28,* 283–285.

Hayden, L. A., & Watson, E. B. (2008). Grain boundary mobility of carbon in Earth's mantle: A possible carbon flux from the core. *Proceedings of the National Academy of Sciences of the USA, 105*(25), 8537–8541.

International Union of Geological Sciences, & Le Maitre, R. W. (1989). *A classification of igneous rocks and glossary of terms: Recommendations of the International Union of Geological Sciences Subcommission on the Systematics of Igneous Rocks*. Oxford: Blackwell.

Irving, A. J., & Wyllie, P. J. (1973). Melting relationships in CaO–CO_2 and MgO–CO_2 to 36 kbar with comments on CO_2 in the mantle. *Earth and Planetary Science Letters, 20,* 220–225.

Isshiki, M., Irifune, T., Hirose, K., Ono, S., Ohishi, Y., Watanuki, T., et al. (2004). Stability of magnesite and its high-pressure form in the lowermost mantle. *Nature, 427*(6969), 60–63.

Ivanov, A. B., & Deutsch, A. (2002). The phase diagram of $CaCO_3$ in relation to shock compression and decomposition. *Physics of the Earth and Planetary Interiors, 129,* 131–143.

Izraeli, E. S., Harris, J. W., & Navon, O. (2001). Brine inclusions in diamonds: A new upper mantle fluid. *Earth and Planetary Science Letters, 187,* 323–332.

Javoy, M. (1997). The major volatile elements of the Earth: Their origin, behavior, and fate. *Geophysical Research Letters, 24,* 177–180.

Kaminsky, F. V. (2012). Mineralogy of the lower mantle: A review of 'super-deep' mineral inclusions in diamond. *Earth-Science Reviews, 110*(1–4), 127–147. doi:10.1016/j.earscirev.2011.10.005

Kaminsky, F., Matzel, J., Jacobsen, B., Hutcheon, I., & Wirth, R. (2016a). Isotopic fractionation of oxygen and carbon in decomposed lower-mantle inclusions in diamonds. *Mineralogy and Petrology, 110*(2–3), 379–385. doi:10.1007/s00710-015-0401-7

Kaminsky, F. V., Ryabchikov, I. D., McCammon, C., Longo, M., Abakumov, A. M., Turner, S., et al. (2015a). Oxidation potential in the Earth's lower mantle as recorded from ferropericlase inclusions in diamond. *Earth and Planetary Science Letters, 417,* 49–56. doi:10.1016/j.epsl.2015.02.029

Kaminsky, F. V., Ryabchikov, I. D., & Wirth, R. (2016b). A primary natrocarbonatitic association in the Deep Earth. *Mineralogy and Petrology, 110*(2–3), 387–398. doi:10.1007/s00710-015-0368-4

Kaminsky, F., Wirth, R., Matsyuk, S., Schreiber, A., & Thomas, R. (2009). Nyerereite and nahcolite inclusions in diamond: Evidence for lower-mantle carbonatitic magmas. *Mineralogical Magazine, 73*(5), 797–816. doi:10.1180/minmag.2009.073.5.797

Kaminsky, F. V., Wirth, R., & Schreiber, A. (2013). Carbonatitic inclusions in Deep Mantle diamond from Juina, Brazil: New minerals in the carbonate-halide association. *The Canadian Mineralogist, 51,* 669–688. doi:10.3749/canmin.51.5.669

Kaminsky, F. V., Wirth, R., & Schreiber, A. (2015b). A microinclusion of lower-mantle rock and some other lower-mantle inclusions in diamond. *Canadian Mineralogist, 53*(1), 83–104. doi:10.3749/canmin.1400070

Katsura, T., Yoneda, A., Yamazaki, D., Yoshino, T., & Ito, E. (2010). Adiabatic temperature profile in the mantle. *Physics of the Earth and Planetary Interiors, 183,* 212–218.

Kiseeva, E. S., Litasov, K. D., Yaxley, G. M., Ohtani, E., & Kamenetsky, V. S. (2013). Melting and phase relations of carbonated eclogite at 9–21 GPa and the petrogenesis of alkali rich melts in the deep mantle. *Journal of Petrology, 54*(8), 1555–1583.

Klein-BenDavid, O., Logvinova, A. M., Schrauder, M., Spetius, Z. V., Weiss, Y., Hauri, E., et al. (2009). High-Mg carbonatitic microinclusions in some Yakutian diamonds: A new type of diamond-forming fluid. *Lithos, 112S,* 648–659.

Klein-BenDavid, O., Wirth, R., & Navon, O. (2006). TEM imaging and analysis of microinclusions in diamonds: A close look at diamond-growing fluids. *American Mineralogist, 91*(2–3), 353–365.

Koch-Müller, M., Jahn, S., Birkholz, N., Ritter, E., & Schade, U. (2016). Phase transitions in the system $CaCO_3$ at high P and T determined by in situ vibrational spectroscopy in diamond anvil cells and first-principles simulations. *Physics and Chemistry of Minerals, 43,* 545. doi:10.1007/s00269-016-0815-8

Kono, Y., Kenney-Benson, C., Hummer, D., Ohfuji, H., Park, C., Shen, G., et al. (2014). Ultralow viscosity of carbonate melts at high pressures. *Nature Communications, 5,* 5091. doi:10.1038/ncomms6091

Kresten, P. (1983). Carbonatite nomenclature. *Geologische Rundschau, 72,* 389–395.

Lay, T., Garnero, E. J., & Williams, Q. (2004). Partial melting in a thermo-chemical boundary layer at the base of the mantle. *Physics of the Earth and Planetary Interiors, 146,* 441–467.

Lin, J.-F., Liu, J., Jacobs, C., & Prakapenka, V. B. (2012). Vibrational and elastic properties of ferromagnesite across the electronic spin-pairing transition of iron. *American Mineralogist, 97,* 583–591.

Litasov, K. D., & Ohtani, E. (2009). Phase relations in the peridotite–carbonate–chloride system at 7.0–16.5 GPa and the role of chlorides in the origin of kimberlite and diamond. *Chemical Geology, 262,* 29–41.

Litasov, K. D., Shatskiy, A., & Ohtani, E. (2013a). Earth's mantle melting in the presence of C-O-H-bearing fluid. In S. Karato (Ed.), *Physics and chemistry of the deep Earth* (pp. 38–65). New York: Wiley-Blackwell.

Litasov, K. D., Shatskiy, A., Ohtani, E., & Yaxley, G. M. (2013b). Solidus of alkaline carbonatite in the deep mantle. *Geology, 41,* 79–82.

Litvin, Y. A. (2009). The physicochemical conditions of diamond formation in the mantle matter: Experimental studies. *Russian Geology and Geophysics, 50,* 1188–1200.

Litvin, Y., Spivak, A., Solopova, N., & Dubrovinsky, L. (2014). On origin of lower-mantle diamonds and their primary inclusions. *Physics of the Earth and Planetary Interiors, 228,* 176–185.

Liu, J., Lin, J.-F., & Prakapenka, V. B. (2015). High-pressure orthorhombic ferromagnesite as a potential deep-mantle carbon carrier. *Scientific Reports, 5,* 7640.

Liu, L., & Lin, C. (1997). A calcite-aragonite-type phase transition in $CdCO_3$. *American Mineralogist, 82,* 643–646.

Luth, R. W. (2001). Experimental determination of the reaction aragonite + magnesite = dolomite at 5 to 9 GPa. *Contributions to Mineralogy and Petrology, 141,* 222–232.

Maeda, F., Ohtani, E., Kamada, S., Sakamaki, T., Hirao, N., & Ohishi, Y. (2017). Diamond formation in the deep lower mantle: A high-pressure reaction of $MgCO_3$ and SiO_2. *Scientific Reports, 7,* 40602. doi:10.1038/srep40602

Mao, Z., Armentrout, M., Rainey, E., Manning, C. E., Dera, P., Prakapenka, V. B., et al. (2011). Dolomite III: A new candidate lower mantle carbonate. *Geophysical Research Letters, 38,* L22303. doi:10.1029/2011GL049519

Matas, J., Bass, J. D., Ricard, Y., Mattern, E., & Bukowinsky, M. S. (2007). On the bulk composition of the lower mantle: Predictions and limitations from generalized inversion of radial seismic profiles. *Geophysical Journal International, 170,* 764–780.

McDonough, W. F. (2003). Compositional model for the Earth's core. In H. D. Holland & K. K. Turekian (Eds.), *Treatise on geochemistry* (pp. 547–568). Oxford: Pergamon.

McNamara, A. K., Garnero, E. J., & Rost, S. (2010). Tracking deep mantle reservoirs with ultra-low velocity zones. *Earth and Planetary Science Letters, 299,* 1–9.

Merlini, M., Crichton, W. A., Chantel, J., Guignard, J., & Poli, S. (2014). Evidence of interspersed co-existing $CaCO_3$-III and $CaCO_3$-IIIb structures in polycrystalline $CaCO_3$ at high pressure. *Mineralogical Magazine, 78*(2), 225–233.

Merlini, M., Crichton, W., Hanfland, M., Gemmi, M., Müller, H., Kupenko, I., et al. (2012b). Structures of dolomite at ultrahigh pressure and their influence on the deep carbon cycle. *Proceedings of the National Academy of Sciences of the U.S.A., 109*, 13509–13514.

Merlini, M., Hanfland, M., & Crichton, W. (2012a). $CaCO_3$-III and $CaCO_3$-VI, high-pressure polymorphs of calcite: Possible host structures for carbon in the Earth's mantle. *Earth and Planetary Science Letters, 333,* 265–271.

Merlini, M. Hanfland, M., Salamat, A., Petitgirard, S., & Müller, H. (2015). The crystal structures of $Mg_2Fe_2C_4O_{13}$, with tetrahedrally coordinated carbon, and $Fe_{13}O_{19}$, synthesized at deep mantle conditions. *American Mineralogist, 100*(8–9), 2001–2004.

Mitchell, R. H. (2005). Carbonatites and carbonatites and carbonatites. *Canadian Mineralogist, 43,* 2049–2068.

Oganov, A. R., Glass, C. W., & Ono, S. (2006). High-pressure phases of $CaCO_3$: Crystal structure prediction and experiment. *Earth and Planetary Science Letters, 241*(1/2), 95–103.

Oganov, A. R., Ono, S., Ma, Y., Glass, C. W., & Garcia, A. (2008). Novel high-pressure structures of $MgCO_3$, $CaCO_3$ and CO_2 and their role in Earth's lower mantle. *Earth and Planetary Science Letters, 273*(1–2), 38–47.

Ono, S., Kikegawa, T., & Ohishi, Y. (2007). High-pressure transition of $CaCO_3$. *American Mineralogist, 92,* 1246–1249.

Pickard, C. J., & Needs, R. J. (2015). Structures and stability of calcium and magnesium carbonates at mantle pressures. *Physical Review B*, *91*,104101. doi:10.1103/PhysRevB.91.104101

Palme, H., & O'Neill, H. S. C. (2003). Cosmochemical estimates of mantle composition. In R. W. Carlson (Ed.), *Treatise on geochemistry (the mantle and core)* (Vol. 2, pp. 1–38). Amsterdam: Elsevier.

Palyanov, Yu N, Shatsky, V. S., Sobolev, N. V., & Sokol, A. G. (2007). The role of mantle ultrapotassic fluids in diamond formation. *Proceedings of National Academy of Sciences USA, 104*(22), 9122–9127.

Panero, W. R., & Kabbes, J. E. (2008). Mantle-wide sequestration of carbon in silicates and the structure of magnesite II. *Geophysical Research Letters, 35,* L14307. doi:10.1029/2008gl034442

Ryabchikov, I. D., & Hamilton, D. L. (1993a). Interaction of carbonate-phosphate melts with mantle peridotites at 20-35 kbar. *South African Journal of Geology, 96,* 143–148.

Ryabchikov, I. D., & Hamilton, D. L. (1993b). Near-solidus carbonate–phosphate melts in mantle peridotites. *Geokhimiya, 12*, 1151–1160.

Ryabchikov, I. D., & Kaminsky, F. V. (2013). Redox potential of diamond formation processes in the lower mantle. *Geology of Ore Deposits, 55*(1), 1–12.

Ryabchikov, I. D., Orlova, G. P., Senin, V. G., & Trubkin, N. V. (1991). Interphase distribution of rare earth elements during partial melting in the system peridotite-carbonate-phosphate. *Geologhiya Rudnykh Mestorozhdeniy, 3*, 78–86 (in Russian).

Safonov, O. G., Kamenetsky, V. S., & Perchuk, L. L. (2011). Links between carbonatite and kimberlite melts in chloride-carbonate-silicate systems: Experiments and application to natural assemblages. *Journal of Petrology, 52,* 1307–1331.

Santillán, J., Katalli, K., & Williams, Q. (2005). An infrared study of carbon-oxygen bonding in magnesite to 60 GPa. *American Mineralogist, 90,* 1669–1673.

Santillán, J., & Williams, Q. (2004a). A high pressure X-ray diffraction study of aragonite and the post-aragonite phase transition in $CaCO_3$. *American Mineralogist, 89,* 1348–1352.

Santillán, J., & Williams, Q. (2004b). A high-pressure infrared and X-ray study of $FeCO_3$ and $MnCO_3$: Comparison with $CaMg(CO_3)_2$-dolomite. *Physics of the Earth and Planetary Interiors, 143–144,* 291–304.

Santillán, J., Williams, Q., & Knittle, E. (2003). Dolomite-II: A high-pressure polymorph of $CaMg(CO_3)_2$. *Geophysical Research Letters, 30*(2), 1054. doi:10.1029/2002GL016018

Schrauder, M., & Navon, O. (1994). Hydrous and carbonatitic mantle fluids in fibrous diamonds from Jwaneng, Botswana. *Geochimica et Cosmochimica Acta, 58,* 761–771.

Scott, H. P., Doczy, V. M., Frank, M. R., Hasan, M., Lin, J.-F., & Yang, J. (2013). Magnesite formation from MgO and CO_2 at the pressures and temperatures of Earth's mantle. *American Mineralogist, 98*(7), 1211–1218.

Seto, Y., Hamane, D., Nagai, T., & Fujino, K. (2008). Fate of carbonates within oceanic plates subducted to the lower mantle, and a possible mechanism of diamond formation. *Physics and Chemistry of Minerals, 35*(4), 223–229.

Sharygin, I. S., Golovin, A. V., Korsakov, A. V., & Pokhilenko, N. P. (2016). Tychite in mantle xenoliths from kimberlites: The first find and a new genetic type. *Doklady Earth Sciences, 467* (1), 270–274. doi:10.1134/S1028334X16030065

Shatskiy, A. F., & Litasov, K. D. (2015). *Formation of carbonates and a mechanism for the migration of carbonate melts through the Earth's mantle* (246 pp). Novosibirsk: Publishing House of the Siberian Branch of the Russian Academy of Sciences. (in Russian).

Shim, S. H., Duffy, T., & Shen, G. (2000). The stability and P–V–T equation of state of $CaSiO_3$ perovskite in the Earth's lower mantle. *Journal of Geophysical Research, 105*(B11), 25955–25968.

Shirasaka, M., Takahashi, E., Nishihara, Y., Matsukage, K., & Kikegawa, T. (2002). In situ X-ray observation of the reaction dolomite = aragonite + magnesite at 900–1300 K. *American Mineralogist, 87*(7), 922–930.

Skorodumova, N. V., Belonoshko, A. B., Huang, L., Anuja, R., & Johansson, B. (2005). Stability of the $MgCO_3$ structures under lower mantle conditions. *American Mineralogist, 90,* 1008–1011.

Smith, E. (2014). *Fluid inclusions in fibrous and octahedrally-grown diamonds* (Ph.D. thesis). University of British Columbia, 195 p.

Sobolev, N. V., Kaminsky, F. V., Griffin, W. L., Yefimova, E. S., Win, T. T., Ryan, C. G., et al. (1997). Mineral inclusions in diamonds from the Sputnik kimberlite pipe, Yakutia. *Lithos, 39,* 135–157.

Solopova, N. A., Dubrovinsky, L., Spivak, A. V., Litvin, Yu A, & Dubrovinskaia, N. (2015). Melting and decomposition of $MgCO_3$ at pressures up to 84 GPa. *Physics and Chemistry of Minerals, 42*(1), 73–81. doi:10.1007/s00269-014-0701-1

Sonin, V. M., Zhimulev, E. I., Chepurov, A. I., & Fedorov, I. I. (2008). Diamond stability in NaCl and NaF melts at high pressure. *Doklady Earth Sciences, 420*(4), 641–643.

Thomson, A. R., Walter, M. J., Lord, O. T., & Kohn, S. C. (2014). Experimental determination of melting in the systems enstatite-magnesite and magnesite-calcite from 15 to 80 GPa. *American Mineralogist, 99,* 1544–1554.

Wang, A., Pasteris, J. D., Meyer, H. O. A., & Dele-Duboi, M. L. (1996). Magnesite-bearing inclusion assemblage in natural diamond. *Earth and Planetary Science Letters, 141*(1–4), 293–306.

Weiss, Y., Kiflawi, I., Davies, N., & Navon, O. (2014). High density fluids and the growth of monocrystalline diamonds. *Geochimica et Cosmochimica Acta, 141,* 145–159.

Wen, L., & Helmberger, D. V. (1998). Ultra-low velocity zones near the core-mantle boundary from broadband PKP precursors. *Science, 279,* 1701–1703.

Wirth, R., Dobrzhinetskaya, L., Harte, B., Schreiber, A., & Green, H. W. (2014). High-Fe (Mg, Fe)O inclusion in diamond apparently from the lowermost mantle. *Earth and Planetary Science Letters, 404,* 365–376.

Wirth, R., Kaminsky, F., Matsyuk, S., & Schreiber, A. (2009). Unusual micro- and nano-inclusions in diamonds from the Juina Area, Brazil. *Earth and Planetary Science Letters, 286*(1–2), 292–303.

Wirth, R., & Rocholl, A. (2003). Nano-crystalline diamond from the Earth mantle underneath Hawaii. *Earth and Planetary Science Letters, 211*(3–4), 357–369.

Wyllie, P. J., & Ryabchikov, I. D. (2000). Volatile components, magmas, and critical fluids in upwelling mantle. *Journal of Petrology, 41,* 1195–1206.

Zaitsev, A. N., & Keller, J. (2006). Mineralogical and chemical transformation of Oldoinyo Lengai natrocarbonatites, Tanzania. *Lithos, 91,* 191–207.

Zaitsev, A. N., Wenzel, T., Vennemann, T., & Markl, G. (2014). Tinderet volcano, Kenya: An altered natrocarbonatite locality? *Mineralogical Magazine, 77*(3), 213–226.

Zedgenizov, D. A., Ragozin, A. L., Kalininaa, V. V., & Kagi, H. (2016). The mineralogy of Ca-rich inclusions in sublithospheric diamonds. *Geochemistry International, 54*(10), 890–900. doi:10.1134/S0016702916100116

Zerr, A., Diegeler, A., & Boehler, R. (1998). Solidus of the Earth's deep mantle. *Science, 281* (5374), 243–246.

Zhang, Y., & Zindler, A. (1993). Distribution and evolution of carbon and nitrogen in Earth. *Earth and Planetary Science Letters, 117,* 331–345.

Zhong, S. (2006). Constraints on thermochemical convection of the mantle from plume heat flux, plume excess temperature, and upper mantle temperature. *Journal of Geophysical Research, 111,* B04409. doi:10.1029/2005JB003972